## Soft Matter



View Article Online **PAPER** 



Cite this: Soft Matter, 2023, 19.9269

Received 29th July 2023, Accepted 19th October 2023

DOI: 10.1039/d3sm01003a

rsc.li/soft-matter-journal

# Effect of temperature on the air-water surface mechanical behavior of water-spread block copolymer micelles†

In the pursuit of the development of a first-in-kind polymer lung surfactant (PLS) therapeutic whose effects are biophysical in nature, a comprehensive understanding of the factors affecting the air-water surface mechanical behavior of water-spread block copolymer micelles is desired. To this end, we explore the effect of temperature on the surface mechanical behavior of two different micelle core chemistries, poly(styrene) (PS) and poly(tert-butyl methacrylate) (PtBMA), each having poly(ethylene glycol) (PEG) as the hydrophilic block. The behavior is characterized using surface pressure-area isotherms and quantitative Brewster angle microscopy. The results indicate that the temperature has a significant effect on the micelle structure at the interface and this effect is related to the core  $T_{\alpha}$  as well as the core interfacial tension properties. When temperature is higher than the core  $T_{\alpha}$  for PS-PEG, the spherical micelle core rearranges to form an oblate-like structure which increases its interfacial area. The structural rearrangement changes the mechanism by which the film produces high surface pressure. For PtBMA-PEG, which has a lower interfacial tension with water and air compared to PS, the core domains spread at the interface when the mobility is sufficiently high such that a PtBMA film is formed under high compression. The implications of these changes on PLS efficacy are discussed highlighting the importance of core  $T_{\alpha}$  characterization for polymer nanoparticle applications.

## 1. Introduction

Our group has recently demonstrated in-depth evidence of the efficacy of using aqueous amphiphilic block copolymer (BCP) micelle solutions as respiratory therapeutics which function by temporarily replacing the native lung surfactant, a substance which reduces the high air-water surface tension  $(\gamma)$  within alveoli, following lung injury. 1,2 The technology, referred to as polymer lung surfactant (PLS), has promising potential to serve as an effective therapeutic for a very deadly condition known as Acute Respiratory Distress Syndrome (ARDS). One of the contributing factors for the high  $(\sim 40\%)^3$  mortality rate for ARDS patients is the dysfunction of native lung surfactant which is a crucial component of the proper respiratory function.<sup>4</sup> The dysfunction occurs because of the presence of surface-active blood proteins which enter into the alveoli due to the increased permeability of alveolar epithelium, the degradation of lung

surfactant phospholipids by phospholipases, and decreased production of lung surfactant by type II alveolar cells.<sup>5</sup> The unique properties of polymer micelle films compared to phospholipid films present an exciting pathway to overcome the shortcomings of previously failed trials of using animalextracted phospholipid surfactants as treatments for ARDS.6

Given that the effect of the PLS is biophysical in nature, the surface mechanical properties of the aqueous surfactant formulation must be carefully considered for optimal efficacy. Specifically, the surfactant formulation ideally should be able to produce high surface pressure ( $\Pi > 60 \text{ mN m}^{-1}$ ), respread well at the interface during repeated compression (exhalation) and expansion (inhalation) cycles, and satisfy the Laplace stability criterion. Preventing Laplace instability is thought to be one of the important roles of lung surfactant. The internal Laplace pressure  $(\Delta P = 2\gamma/R)$  is inversely proportional to the radius (R) of the alveoli; therefore, if  $\gamma$  is not controlled properly, the smaller alveoli will experience higher Laplace pressures causing them to preferentially deflate and collapse.<sup>7</sup> Since natural lung surfactant is designed to decrease surface tension with decreasing surface area in a way which eliminates Laplace instabilities (*i.e.*, ensuring  $\partial(\Delta P)/\partial R > 0$ ), <sup>7</sup> it is important to understand the PLS formulation's ability to prevent Laplace instability. Also, it is important to reiterate that we are

<sup>&</sup>lt;sup>a</sup> Davidson School of Chemical Engineering, Purdue University, West Lafayette, IN 47907, USA. E-mail: yywon@purdue.edu

<sup>&</sup>lt;sup>b</sup> Department of Polymer Science and Engineering, Dankook University, Yongin, Gyeonggi 16890, Republic of Korea

<sup>&</sup>lt;sup>c</sup> Purdue University Institute for Cancer Research, West Lafayette, IN 47907, USA

<sup>†</sup> Electronic supplementary information (ESI) available. See DOI: https://doi.org/

concerned with the surface mechanical properties of waterspread polymer micelles and not that of the organic solventspread block copolymer solutions. Previously, we have shown that  $\sim 5$  kDa +  $\sim 5$  kDa poly(styrene-block-ethylene glycol) (PS-PEG) is well suited for the PLS application. Furthermore, for block copolymer micelles of different sizes but composed of the same PS-PEG polymer, micelles with larger spherical size and higher PEG grafting density are most effective at producing maximum surface pressure (i.e., 72 mN m<sup>-1</sup> at 25 °C).8 Additionally, for other block copolymers also having PEG as the hydrophilic block, hydrophobic blocks with high contact angles and high bulk glass transition temperatures have the most desirable surface mechanical properties.<sup>9</sup>

For amphiphilic block copolymer Langmuir films, commonly formed by spreading polymer chains molecularly dissolved in an organic solvent onto the water surface, the glassy nature of the polymer film has been identified as an important feature for the film to produce a steep rise in surface pressure during compression. 10-13 For example, a Langmuir film of poly(lactic acid-co-glycolic acid)(PLGA)(18 kDa)-PEG(5 kDa) which has an estimated PLGA  $T_{\rm g}$  of 296 K, shows a steep rise in surface pressure at 288 K but not at 298 K due to the film becoming non-glassy.10 However, in the case of water-spread polymer micelles, it is not straightforward to predict what will happen when the temperature is raised such that the core transitions from the rigid glassy state to the rubbery non-glassy state because the core domains are surrounded by a dense PEG corona layer in the micelle state. Additionally, the rigid to rubbery transition for micelle cores is more gradual due to there being a spectrum of  $T_g$  values within the core domain. <sup>14,15</sup> Herein, we study the air-water surface mechanical behavior of water-spread PS-PEG and PtBMA-PEG micelles at various temperatures above and below their respective core  $T_{\rm g}$  values. The core T<sub>o</sub> values were previously characterized by both an <sup>1</sup>H NMR technique<sup>16</sup> (which predicts the core  $T_g$  of the outer core domain) and a molecular rotor technique14 (which predicts the mean core  $T_g$  of the entire core volume). The surface mechanical behavior is characterized using Langmuir trough surface pressure-area isotherms as well as quantitative Brewster angle microscopy (QBAM). The results indicate that the temperature has a significant impact on the behavior of the micelle film, and the behavior depends on the core  $T_{\rm g}$  as well as the air-water interfacial properties of the core domain. These findings are especially important given the proximity of  $T_g$  of the core domains to physiological temperature such that the  $T_g$  of the core domain needs to be considered even for hydrophobic blocks with bulk  $T_g$  values well above physiological temperature.

## 2. Experimental section

### 2.1 Polymer materials

PS(5.2 kDa)-PEG(5.5 kDa) was purchased from Polymer Source, Inc., and was synthesized using living anionic polymerization. PtBMA(5.4 kDa)-PEG(5.0 kDa) was synthesized using reversible addition-fragmentation chain transfer polymerization (RAFT).

PEG(5.0 kDa) (Sigma) was conjugated to the RAFT agent, 4-cyano-4-[(dodecylsulfanylthiocarbonyl)sulfanyl]pentanoic (CDSP) followed by subsequent PtBMA polymerization.

#### 2.2 Polymer characterizations

The number-average molecular weight of the RAFT-synthesized PtBMA-PEG was determined by <sup>1</sup>H NMR using a Bruker Avance III 800 MHz spectrometer. The measurements were done in deuterated chloroform at a concentration of 5 wt%. The polydispersity indices were determined using gel permeation chromatography (GPC) using a Waters 1515 isocratic pump equipped with Styragel HR 4 and Ultrastyragel columns. The mobile phase was THF, and the flow rate was 1 mL min<sup>-1</sup>. Calibration was done using polystyrene standards.

#### 2.3 Micelle formulation

Equilibration-nanoprecipitation (ENP) was used to formulate micelles.8 An initial solvent composition of 30% water + 70% acetone was used followed by equilibration and removal of acetone by dialysis.

### 2.4 Surface pressure-area ( $\pi$ -A) isotherms

A KSV 5000 Langmuir trough (54 cm × 15 cm, 1.4 L subphase volume) and KSV NIMA (54 cm  $\times$  15 cm, 0.7 L subphase volume) were used for surface pressure-area isotherm measurements. The trough had a heating/cooling water jacket embedded underneath, which was connected to a circulating water bath. The temperature of the water subphase was monitored using a thermocouple. Milli-Q-purified water (18 M $\Omega$  cm resistivity) was used as the subphase solvent which has a surface tension of 72 mN m<sup>-1</sup> at 25 °C. A completely wetted filter paper plate, Whatman CHR1 chromatography paper, with 1 cm dry width was used as the Wilhelmy plate. Due to swelling of the filter paper, the true perimeter of the water saturated filter paper was calibrated by using the known value of the air-water surface tension at 25 °C.8 Before each measurement, the trough and the barriers were washed three times with water and ethanol. The cleanliness of the surface was checked by ensuring that a complete compression of the pristine water surface did not lead to a change in surface pressure of more than 0.2 mN m<sup>-1</sup>. Polymers were spread at the air-water interface by placing droplets of the polymer solution uniformly across the water surface using a micro syringe. Typically, 50-100 μL of a 5 mg mL<sup>-1</sup> PS-PEG solution in water was spread onto a trough with an initial area of 810 cm<sup>2</sup>.

#### Dynamic light scattering (DLS)

The hydrodynamic diameters of the block copolymer micelles were measured at 25 °C by DLS using a Brookhaven ZetaPALS instrument. The scattering intensities were measured using a 659 nm laser at a scattering angle of 90°. The hydrodynamic diameters were calculated from the measured diffusion coefficients using the Stokes-Einstein equation. For DLS measurements, the samples were diluted to guarantee single scattering and were filtered with 0.45 µm syringe filters to remove contaminants.

Paper

#### 2.6 Transmission electron microscopy (TEM)

Soft Matter

TEM specimens were prepared by placing 20  $\mu$ L of a 0.01–0.05 mg mL $^{-1}$  polymer micelle solution on a carbon-coated copper TEM grid (pre-treated using an  $O_2$  plasma cleaner to make surface more hydrophilic). A total of 10  $\mu$ L of a 2% uranyl acetate solution was added to the sample solution already placed on the TEM grid, and the mixture was blotted using filter paper and dried. The samples thus prepared were imaged using a 200 kV FEI Tecnai 20 TEM instrument. The TEM images were analyzed using ImageJ software.

#### 2.7 Brewster angle microscopy (BAM)

BAM images were taken using Accurion Ultrabam with a lateral resolution of 2  $\mu$ m and a field of view (FOV) of 800  $\mu$ m  $\times$  430  $\mu$ m equipped with KSV NIMA Langmuir trough which recorded surface pressure data simultaneously to BAM measurements. The measurements were taken during compression of the monolayer at 30 mm min<sup>-1</sup>.

## 3. Results and discussion

#### 3.1 Micelle formulation and characterization

PS-PEG and PtBMA-PEG micelle solutions were prepared by ENP method using formulation conditions of 30% water/70% acetone followed by removal of acetone using dialysis tubing. Various properties of the polymer materials and polymer micelles post acetone removal are shown in Table 1, and TEM images are shown in Fig. S1 in ESI.†

The  $T_g$  of the core domains were characterized previously by two different techniques which provide slightly different insights into the  $T_g$  of the micelle core. The two techniques are described in more detail in separate manuscripts. 14,16 The first technique is the use of the molecular rotor, farnesyl-(2-carboxy-2-cyanovinyl)-julolidine (FCVJ), to measure local viscosity/free volume changes in the core domain. The FCVJ compound is encapsulated in the core domain and the fluorescence is measured as a function of temperature. Given that FCVJ is a very hydrophobic compound, it is expected that the mean core  $T_g$  from FCVJ is expected to reflect the  $T_g$  of the inner core domain. However, since the radial location of the FCVJ molecule is not the same for every micelle, the FCVJ is best fit to a range of core  $T_{\rm g}$  values (which are functions of radial position  $^{15})$  with the mean  $\pm$  range values being reported in Table 1. The other technique uses  $T_2$  <sup>1</sup>H NMR measurements to characterize the local dynamics of PEG chains near the hydrophobic core as a function of temperature. The discontinuity of the core behavior at  $T_{\rm g}$  leads to a discontinuity in the Arrhenius

 $T_2$  behavior of PEG corona chains near the core. Therefore,  $T_2$  <sup>1</sup>H NMR is expected to measure the  $T_g$  of the outer micelle core.

For both micelle core chemistries, the micelle core  $T_{\rm g}$  is significantly suppressed compared to that of the bulk material. For PtBMA, the bulk  $T_{\rm g}$  is 103 °C (calculated using the Flory–Fox equation for  $M_{\rm n}=6.5$  kDa) and the measured  $T_{\rm g}$  from  $T_2$  <sup>1</sup>H NMR is 28 °C and from FCVJ is 33 °C; for PS, the bulk  $T_{\rm g}$  is 81 °C (calculated using the Flory–Fox equation for  $M_{\rm n}=5.2$  kDa) and the measured  $T_{\rm g}$  from  $T_2$  <sup>1</sup>H NMR is 32 °C and from FCVJ is 41 °C. The greater suppression of PtBMA is thought to be related to its lower interfacial tension with water compared to PS. Therefore, water has a greater plasticization effect on PtBMA than on PS. The suppression of micelle core  $T_{\rm g}$  below physiological temperature of 37 °C makes the effective core  $T_{\rm g}$  a relevant parameter to study for the lung surfactant application.

# 3.2 Effect of temperature on the generation of surface pressure for water-spread block copolymer micelles

A detailed surface mechanical analysis of the effect of temperature was done by conducting simultaneous surface pressurearea isotherms and quantitative Brewster angle microscopy (QBAM) of water-spread micelles. For the initial study shown in Fig. 1 and 3, the spreading conditions of 50  $\mu L$  of 5 mg mL $^{-1}$  were used. This spreading amount is below the saturation limit for micelles which minimizes the loss of micelles from the surface and allows for a more direct comparison between temperatures while still being a sufficiently high concentration to examine the behavior at moderate surface pressures.

The current explanation of the generation of surface pressure for micelles with highly hydrophobic and rigid core domains (i.e., PS-PEG and PtBMA-PEG at temperatures below core  $T_{\alpha}$ ) is the following. The initial surface pressure increase (in the surface area range of  $\sim 800-600 \text{ cm}^2$ ) is due interaction of adsorbed PEG chains in the 2D semi dilute concentration regime which can stretch to distances much larger than the bulk hydrodynamic diameter. As the area per micelle values approach the hydrodynamic area ( $\approx \pi D_{\rm h}^2/4$ , which corresponds to 205 cm<sup>2</sup> for the PS-PEG case (Fig. 1) and 278 cm<sup>2</sup> for the PtBMA-PEG case (Fig. 3)), the surface becomes saturated with PEG chains, forming a 2D "concentrated" layer. Consequently, the surface pressure approaches the equilibrium value for a PEG film ( $\Pi_{\rm e,PEG} \cong 10~{\rm mN~m^{-1}}$ ). This surface pressure plateau, corresponding to  $\Pi_{e,PEG}$ , represents the region in which PEG undergoes a transition from the adsorbed to the desorbed state. This transition is akin to the "pancake-to-cigar" (or "pancake-to-mushroom") transition as described in the polymer air-water interface literature. 13,18 Further compression to area per micelle values less than that of the hydrodynamic area causes overlap of neighboring coronas in the subphase such

Table 1 Properties of block copolymer materials and block copolymer micelles used in the study

Polymer (A-B)	$M_{ m n,A}$ (g mol <sup>-1</sup> )	$M_{ m n,B}$ (g mol <sup>-1</sup> )	PDI	A block $T_{g,\text{bulk}}$ (°C)	Micelle core $T_{g,NMR}$ (°C)	Micelle core $T_{g,FCVJ}$ mean (°C)	Micelle core $T_{g,SP}$ (°C)	γ <sub>A-water</sub> (mN m <sup>-1</sup> )	$\begin{pmatrix} \gamma_{\text{A-air}} \\ (\text{mN m}^{-1}) \end{pmatrix}$	D <sub>c</sub> (nm)	D <sub>h</sub> (nm)
PS-PEG	5200	5500	1.11	81	32	$41 \pm 24 \\ 33 \pm 11$	36	39	41	18.4	33.5
PtBMA-PEG	6500	5000	1.19	103	28		27	25	31	17.1	32.8

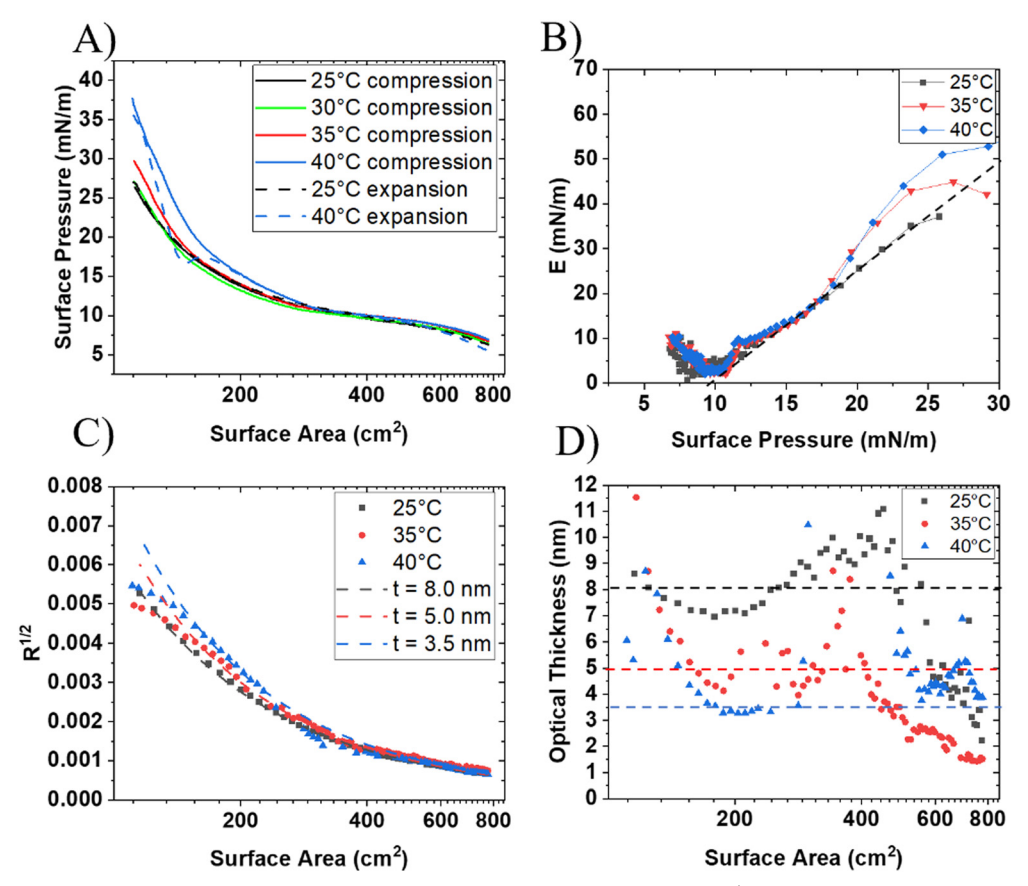


Fig. 1 (A) Surface pressure—area isotherms for water-spread PS-PEG micelles (50  $\mu$ L of 5 mg mL $^{-1}$  solution) compressed at 30 mm min $^{-1}$  at various temperatures. Solid lines represent compressions, and dashed lines represent expansions. (B) Modulus,  $E = -A \frac{\mathrm{d}\Pi}{\mathrm{d}A'}$  plots as a function of surface pressure. The slope of the dashed line represents the y value (= 2.25) used in the de Gennes scaling analysis. (C) Reflectivity as a function of surface area measured simultaneously with surface pressure-area isotherm. Dashed lines represent constant thickness and mass model using t = 8, 5 and 3 nm. (D) Estimated thickness from solving eqn (1) and (2) using constant and equal mass

that PEG coronas exist in 3D semi-dilute regime PEG sublayer. This causes the accumulation of osmotic pressure and the pressure continues to rise until the micelle core domains come into close contact causing collapse of the micelle monolayer which typically occurs at high surface pressures (> 60 mN m<sup>-1</sup>).<sup>8,9</sup>

The surface pressure-area isotherms for PS-PEG micelles at various subphase temperatures above and below the respective core  $T_g$  values are shown in Fig. 1(A). When the temperature of the subphase is raised to 35 °C and 40 °C, there is a clear upward shift in the isotherm to higher surface pressures once the monolayers are compressed beyond  $\Pi_{e,PEG}$ . The modulus  $(E = -A \frac{d\Pi}{dA})$  plots (Fig. 1(B)) show that for the 25 °C case there is a linear relationship between the modulus and surface pressure above  $\Pi_{e,PEG}$ ;  $\Pi_{e,PEG}$  can be visualized by the local minimum in the modulus plots at approximately 10 mN m<sup>-1</sup>. The de Gennes scaling for osmotic pressure predicts that  $E = y\Pi$  where y = dv/(dv)-1), d is the dimensionality, and  $\nu$  is the Flory exponent. <sup>19-21</sup> Using d = 3, the 25 °C modulus plot for  $\Pi > 10$  mN m<sup>-1</sup> gives a Flory exponent of v = 0.60 (y = 2.25) which agrees well with reported value for PEG in water of  $\nu = 0.58$ .<sup>22</sup> The value of d = 3 is employed because the increase in surface pressure is attributed to

the osmotic pressure resulting from the overlapping PEG corona layers in the subphase. These layers behave as if they are in the 3D semi-dilute regime, as illustrated in the upper panel of Fig. 2. It is important to note that when  $\Pi > \Pi_{e,PEG}$ , the 2D adsorbed PEG chains have already attained a "concentrated" state. Consequently, within this region, compression does not entail the development of osmotic pressure within the 2D adsorbed PEG layer. For the 40 °C case, the modulus sharply increases at around 17 mN m<sup>-1</sup> and deviates from the linear osmotic pressure scaling relationship indicating that the surface pressure buildup is no longer due to the PEG 3D osmotic pressure alone.

The monolayer properties were further examined by QBAM which measures the reflectivity (R) of the film at the Brewster angle of water (53°) as a function of surface area. The reflectivity from QBAM can be related to the optical thickness of the film (t) and the refractive index of the film  $(n_f)$  through eqn (1) where  $\lambda$  is the incident wavelength (650 nm) and  $n_{\rm w}$  is the refractive index of water<sup>23</sup>

$$R^{1/2} = \frac{\pi t}{\lambda} \frac{n_{\rm f}^2 - n_{\rm w}^2 - 1 + (n_{\rm w}/n_{\rm f})^2}{(1 + n_{\rm w}^2)^{1/2}} \tag{1}$$

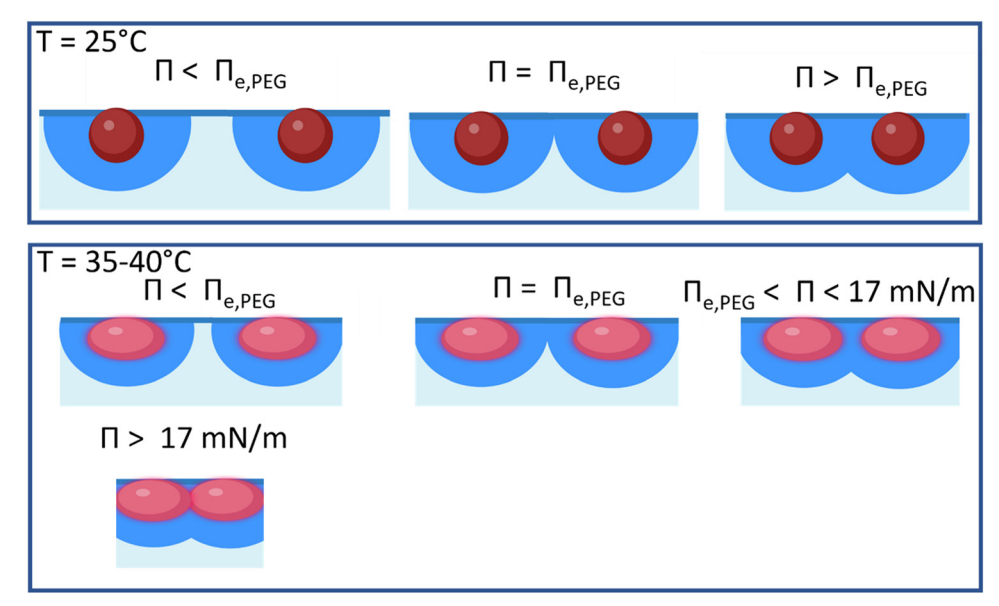


Fig. 2 Schematic illustration of the effect of temperature on the proposed PS-PEG micelle surface structure at different surface pressures during compression after spreading of 50  $\mu L$  of 5 mg mL $^{-1}$  solution.

Furthermore,  $n_f$  can be estimated by eqn (2) where M is the mass of the film,  $\frac{dn}{dc}$  is the refractive index increment, and A is the total surface area

$$n_{\rm f} = n_{\rm w} + \frac{{\rm d}n}{{\rm d}c} \frac{M}{At} \tag{2}$$

For insoluble films with rigid core domains, it is expected that M and t will remain constant during compression. Plots of the square root of reflectivity  $(R^{1/2})$  as a function of surface area for the 25 °C, 35 °C and 40 °C cases along with examples of constant M and t fits to the respective reflectivity curves are shown in Fig. 1(C).

For the fits, it was assumed that the mass (M) of the film was the same for each case. For the 25  $^{\circ}$ C case ( $T < \text{core } T_{\sigma}$ ), the reflectivity data is fit well to a constant thickness model of t =8 nm for the entire range of surface area (A). This thickness is about half of the micelle core diameter, and this is thought to be because the micelle cores are submersed in water and the micelle film contains water in the interstitial regions of the film. For the 35 °C and 40 °C case, the  $R^{1/2}$  values increase more rapidly with decreasing surface area in the range from 400 to 170 cm<sup>2</sup>. The more rapid increase in  $R^{1/2}$  suggests a decreased film thickness as shown by the constant thickness plots of t =5 nm and t = 3 nm. However, the constant thickness plots fail to describe the data well once the monolayer area is compressed to less than 170 cm<sup>2</sup> for the 40 °C case and 150 cm<sup>2</sup> for the 35 °C case. These area values both correspond to a surface pressure of  $\sim$  17.5 mN m<sup>-1</sup> which is the same surface pressure at which the modulus deviates from the linear osmotic pressure scaling relationship suggesting there is a direct relationship between these two phenomena.

The reflectivity data were further analyzed by directly solving for the thickness values as a function of surface area, instead of using the constant thickness model, and these results are shown in Fig. 1(D). Using scaling analysis of eqn (1) with respect to t, it can be shown that  $R^{1/2} \sim t \cdot \left(n_{\rm f}^2 + \left(\frac{n_{\rm w}}{n_{\rm f}}\right)^2\right)$ . Since  $n_{\rm f} > n_{\rm w}$ , the scaling reduces to  $R^{1/2} \sim t \cdot (n_{\rm f}^2)$ . Scaling analysis of eqn (2) shows  $n_{\rm f} \sim \frac{1}{t}$ . Combining both,  $R^{1/2} \sim \frac{1}{t}$ . Therefore, there is one solution when solving for t directly. For the 25 °C case, when the film is compressed below 350 cm<sup>2</sup> (which corresponds to surface pressures greater than  $\Pi_{e,PEG}$  = 10 mN m<sup>-1</sup>), the calculated thickness values oscillate around the value of t = 8 nm which was shown to model the data well in Fig. 1(C). However, at larger surface areas the calculated thicknesses deviate significantly from the t = 8 nm value. This indicates that the QBAM model used in this study is not accurate when the micelles are at low surface coverages. For the 35 °C and 40 °C cases below 350 cm<sup>2</sup>, the thickness values remain relatively constant around t = 5 nm and t = 3 nm, respectively, until the area is decreased below 200 cm<sup>2</sup> at which point the thickness values increase to values closer to the 25  $^{\circ}\mathrm{C}$ case. Therefore, the deviation from the constant thickness model at low surface area in Fig. 1(C) indicates an increase in thickness in the micelle film.

Based on the previous results, the following hypothesis (depicted in Fig. 2) is proposed for the effect of temperature on the surface mechanical behavior of PS-PEG micelles. When the temperature is raised above the core outer  $T_g$ , the spherical micelle structure rearranges at the interface to form an oblatelike structure which maximizes the contact of the micelle core with air and also the contact of PEG with the air-water interface. This change in structure results in an increase in the

cross-sectional area of the micelle compared to that of the spherical  $\pi D_h^2/4$  value. Therefore, since the oblate micelles occupy a larger interfacial area, the surface pressure rise occurs at larger surface areas compared to that of the below  $T_g$  case. Additionally, the change to the oblate structure results in a decrease in the vertical thickness of the micelle structure which is consistent with the QBAM thickness values above  $\sim 200 \text{ cm}^2$ . Lastly, the increase in interfacial area occupied by the PS domains causes the domains to come into contact at larger areas compared to that for the non-changed spherical cores. Therefore, at 17.5 mN m<sup>-1</sup> the increase in modulus and the increase in thickness are caused by the contact and deformation of the core domains such that the surface pressure increase is no longer from the PEG osmotic pressure alone. The core domains are sufficiently rigid to produce a continued rise of surface pressure which is likely due to the internal core  $T_{g}$  measured from FCVJ being greater than 40 °C.

The same set of measurements were carried out for water-spread PtBMA-PEG micelles, and the results are shown in Fig. 3. The isotherm results, shown in Fig. 3(A), show markedly different behavior than the PS-PEG case. First, when the temperature is raised to just above core  $T_{\rm g}$  (30 and 35 °C),

the isotherms are shifted to slightly higher surface pressures in the 200–400  $\rm cm^2$  area range; however, the isotherms have a lower modulus at surface pressures greater than about 10 mN m $^{-1}$  and are thus shifted downward at areas below 200 cm $^2$ . Furthermore, when the temperature is raised to 40  $^{\circ}$ C, the isotherm shows remarkably different behavior as there is a much more rapid increase in surface pressure in the 200–400 cm $^2$  range. Additionally, the 40  $^{\circ}$ C isotherm shows the presence of a secondary pseudo-plateau at around 25 mN m $^{-1}$ .

To gain more information on the changes observed in the isotherms, QBAM analysis was done in the same manner as for PS-PEG. The  $R^{1/2}$  values for the 20 °C, 35 °C and 40 °C cases are shown in Fig. 3(B) along with constant thickness plots for t=0.5, 6 and 20 nm at the same film mass (M). Similar to the PS-PEG case at 25 °C, the PtBMA-PEG compression at 20 °C fits well to a constant thickness of t=6 nm. For the 35 °C case, although the  $R^{1/2}$  values are initially higher when the PEG plateau is reached near 400 cm², the  $R^{1/2}$  increases less rapidly and is shifted downward compared to the 20 °C case such that in the low surface area regime the  $R^{1/2}$  plots is fit well by a constant thickness of t=20 nm. For the 40 °C case, the  $R^{1/2}$  increases much more rapidly and fits well

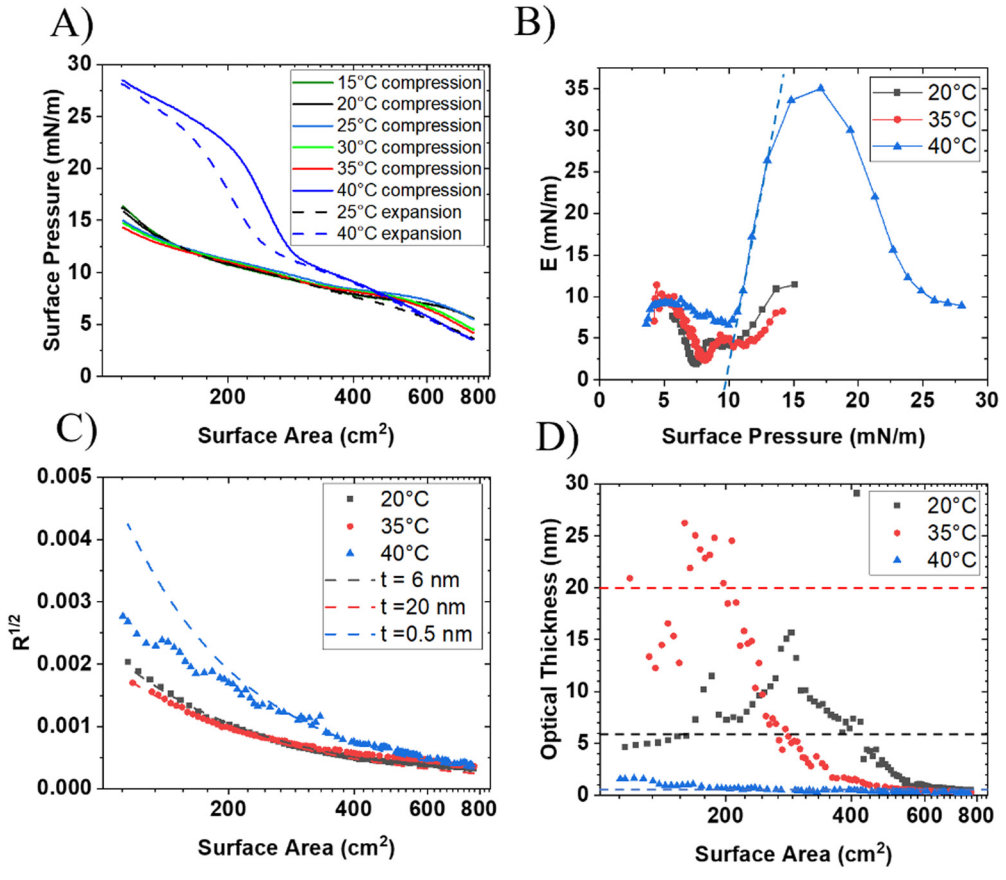


Fig. 3 (A) Surface pressure—area isotherms for water-spread PtBMA-PEG micelles (50  $\mu$ L of 5 mg mL<sup>-1</sup> solution) compressed at 30 mm min<sup>-1</sup> at various temperatures. Solid lines represent compressions, and dashed lines represent expansions. (B) Modulus,  $E = -A \frac{d\Pi}{dA}$ , plots as a function of surface pressure. The slope of the dashed line represents the y value (8.1) used in the de Gennes scaling analysis. (C) Square root of reflectivity as a function of surface area measured simultaneously with surface pressure—area isotherm. The dashed lines represent constant thickness and mass model using t = 6, 20 and 0.5 nm. (D) Estimated thickness from solving eqn (1) and (2) using constant and equal mass.

to a thickness of t = 0.5 nm for surface areas greater than around 200 cm<sup>2</sup>.

The thickness values were directly solved for as a function of surface area, and the resulting plots are shown in Fig. 3(D). For the 20 °C case, when the film is compressed below 250 cm<sup>2</sup> (which corresponds to surface pressures greater than  $\Pi_{e \text{ PFG}}$  = 10 mN m<sup>-1</sup>) the thickness values fluctuate around the value of t = 6 nm which was shown to model the data well in Fig. 3(C). The peak at 180 cm<sup>2</sup> is a result of noise in the reflectivity data. As seen for the PS-PEG case, the QBAM-calculated thickness trends are less reliable at large surface areas. For the 35 °C case, compression below 250 cm<sup>2</sup> causes a rapid increase in thickness such that the estimated thickness is about double that of the 20 °C case. For the 40 °C case, the estimated thickness remains around 0.5 nm in the area range of 200-400 cm<sup>2</sup>. When the area is reduced below 200 cm2, the thickness roughly doubles to near 1 nm.

Based on the previous results, the following hypothesis (depicted in Fig. 4) is proposed for PtBMA-PEG micelles. When temperature is at or slightly above outer core  $T_g$ , the micelles arrange to form oblate-like structures just like for the PS-PEG case. However, PtBMA-PEG micelles at 30 and 35 °C deform rapidly and possibly fuse when compressed due to internal core  $T_g$  also being below 30 °C. Therefore, the modulus is lowered, and the thickness rapidly increases when compressed above 10 mN m<sup>-1</sup>. When the temperature is sufficiently high (i.e., 40 °C), the combination of the fluidlike core domain and

the PtBMA having a positive spreading coefficient ( $s \equiv \gamma_{air-water}$  –  $(\gamma_{\text{PtBMA-air}} + \gamma_{\text{PtBMA-water}})^{24} = 72 - (31 + 25)^{25,26} = 16 \text{ mN m}^{-1} \text{ at}$ 25 °C; the combined interfacial tension of PtBMA-air and PtBMA-water is less than that of air-water) causes the micelle structure to dissociate to form a planar structure with PtBMA wetting the air-water interface and PEG extending into the water subphase. The planar PtBMA film has a much lower thickness than the PtBMA-PEG micelle structure as reflected by the order of magnitude decrease in the optical thickness from QBAM.

The interpretation of PtBMA forming a continuous film when PtBMA-PEG micelles are spread at 40 °C is supported by several pieces of evidence. Firstly, the surface pressure at the onset of the pseudo-plateau (~25 mN m<sup>-1</sup>) coincides reasonably well with the spreading coefficient of PtBMA (16 mN m<sup>-1</sup>). Since surface pressure  $(\Pi)$  is the difference between the surface tension of the clean interface ( $\gamma_o \equiv \gamma_{air-water}$ ) and surfactantcovered interface  $(\gamma)$  and the surface tension of a continuous PtBMA film is predicted to be  $\gamma = \gamma_{PtBMA-air} + \gamma_{PtBMA-water}$ , the predicted surface pressure when a PtBMA film is formed is  $\Pi = \gamma_{o} - \gamma = \gamma_{air-water} - (\gamma_{PtBMA-air} + \gamma_{PtBMA/water}) = s$ . It should be noted s is an inherent property of the polymer material and does not depend on concentration; only when the polymer forms a continuous film would  $\Pi$  be expected to be equal to s. Previous reports have demonstrated a plateau for PtBMA homopolymers at 18 mN m<sup>-1</sup>;<sup>27</sup> the slightly elevated plateau for PtBMA-PEG is consistent with there being an additional surface

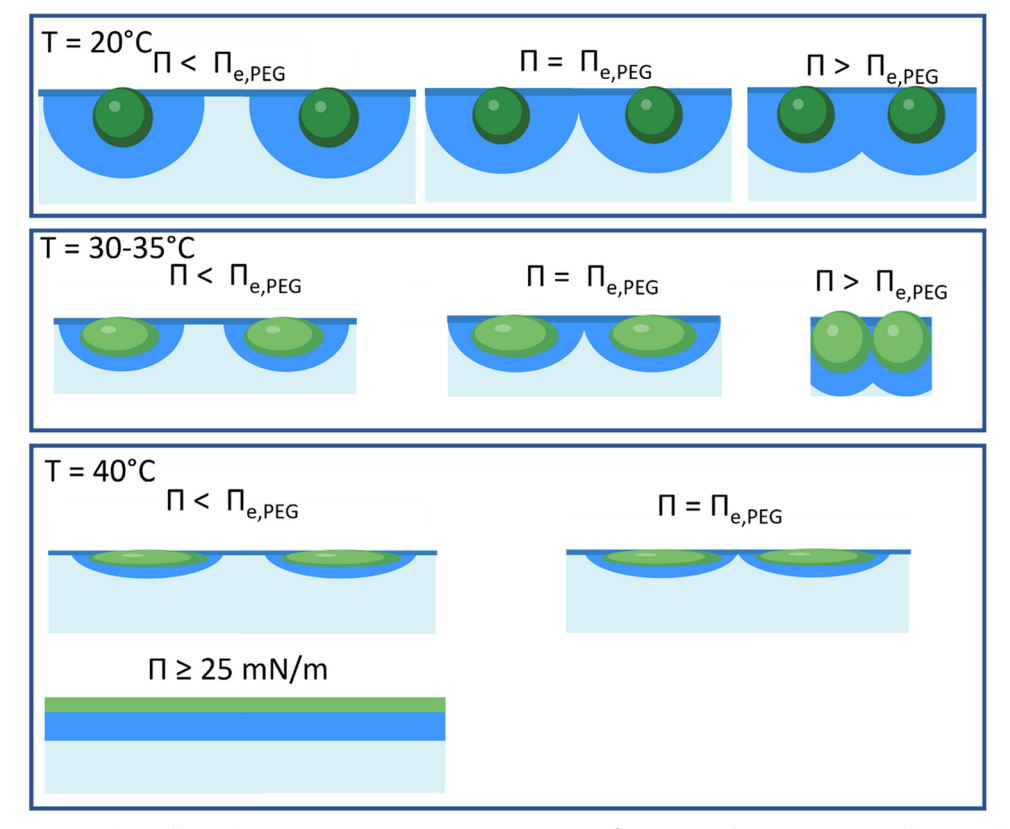


Fig. 4 Schematic illustration of the effect of temperature on the proposed PtBMA-PEG micelle surface structure at different surface pressures during compression after spreading of 50  $\mu$ L of 5 mg mL $^{-1}$  solution.

tension reduction by the PEG chains in the subphase. 28,29 Lastly, there is a much steeper rise in surface pressure above  $\Pi_{\text{e.PEG}}$  which is inconsistent with an osmotic pressure increase in the 3D PEG corona sublayer. Assuming the 3D form of the de Gennes scaling relationship for osmotic pressure (d = 3), the calculated 3D Flory exponent for the 40 °C case in the 10-15 mN m<sup>-1</sup> surface pressure range is  $\nu = 0.38$  ( $\nu = 8.1$ ), and this value would mean the PEG sublayer is in the fully collapsed state which is unphysical for the hydrophilic PEG chains at 40 °C. The surface pressure increase in this range is likely due to the replacement of PEG chains with PtBMA chains at the interface. Although the PtBMA is proposed to form a continuous film at the air-water interface, the area per monomer value ( $\sim 4 \text{ Å}^2$ ) at the onset of the pseudo-plateau (shown in Fig. S2 in ESI†) is much lower than a previously reported value for the air-water interfacial area occupied by a PtBMA monomer ( $\sim 22 \text{ Å}^2$ ) in a single-monomer-thick monolayer<sup>27</sup> which suggests that PtBMA blocks form a film several monomers thick at the air-water interface under these conditions.

Given the ability of the core domain of PtBMA-PEG micelles to spread at the interface at 40 °C, we investigated whether this transition can be also achieved by repeated compression and expansion cycles at temperatures below 40 °C. Therefore, the repeated compression and expansion isotherms and QBAM measurements were taken at 35 °C. The compression curves are shown in Fig. 5(A), and they show that there is a systematic shift to a higher maximum surface pressures over 6 compression/expansion cycles until the 7th cycle where there is no significant further change. The 7th compression isotherm is very similar to that of the isotherm obtained at 40 °C. Also, the QBAM reflectivity data were compared between the 1st and 7th cycle and are shown in Fig. 5(B). The repeated compression and expansion cycles induced a large upward shift in the  $R^{1/2}$  values and thus a reduction in optical thickness also similar to what was seen for the 40 °C case. Therefore, it is reasonable to conclude that repeated compression and expansion of nonglassy PtBMA core domains leads to the fusion and respreading of the PtBMA domains at the air-water interface.

In contrast, PS-PEG micelles do not show this behavior and only show a slight downward shift in maximum surface pressure (Fig. 6(A)) which is either due to loss of mass from the interface or unrelaxed deformation of micelles. Since the sum of PS-water and PS-air interfacial tensions are greater than that of air-water ( $s = \gamma_{\text{air-water}} - (\gamma_{\text{PS-air}} + \gamma_{\text{PS-water}}) = 72 - (41 + 39) = -8 \,\text{mN m}^{-1}$  at 20 °C), <sup>25,26</sup> the formation of a continuous PS film is not thermodynamically favorable.

# 3.3 Use of measurement of surface pressure at constant area during heating to detect core $T_g$ of block copolymer micelles

Although PS-PEG and PtBMA-PEG showed differences in surface mechanical behavior during compression when the temperature is above core outer and internal  $T_g$ , both showed the similar characteristic of the core domain expanding its interfacial area when temperature reaches the outer core  $T_g$ . Therefore, a method was proposed to examine whether this transition could be detected during a constant area temperature sweep. The idea of this measurement is that if micelles are highly compressed, the change in micelle structure because of the core outer  $T_g$  will induce a detectable change in surface pressure with respective to temperature at this point. Therefore, micelles were spread on the interface at 15 °C, compressed to  $25.5 \text{ mN m}^{-1}$ , and then the surface pressure of the micelle film was measured while heating the subphase from 15  $^{\circ}\text{C}$  to 45  $^{\circ}\text{C}$ at a heating rate of 1  $^{\circ}$ C min $^{-1}$  while keeping the area fixed. The raw surface pressure values were adjusted by accounting for the change in surface tension of water with temperature.

The results of the previously described method for the PS-PEG and PtBMA-PEG micelle films are shown in Fig. 7. For both systems, there exists a local minimum near their respective outer core  $T_{\rm g}$  values from  $T_{\rm 2}$  <sup>1</sup>H NMR. The  $T_{\rm g,SP}$  values (core glass transition temperature from surface pressure measurement) were estimated from the plots of the first derivative of surface pressure with respect to temperature (Fig. S3 in ESI†) as the point where the derivative is equal to zero; the values (listed in Table 1) are 36 °C for PS-PEG and 27 °C for PtBMA-PEG. The reason for the local minimum at  $T_{\rm g,SP}$  is as follows. The surface

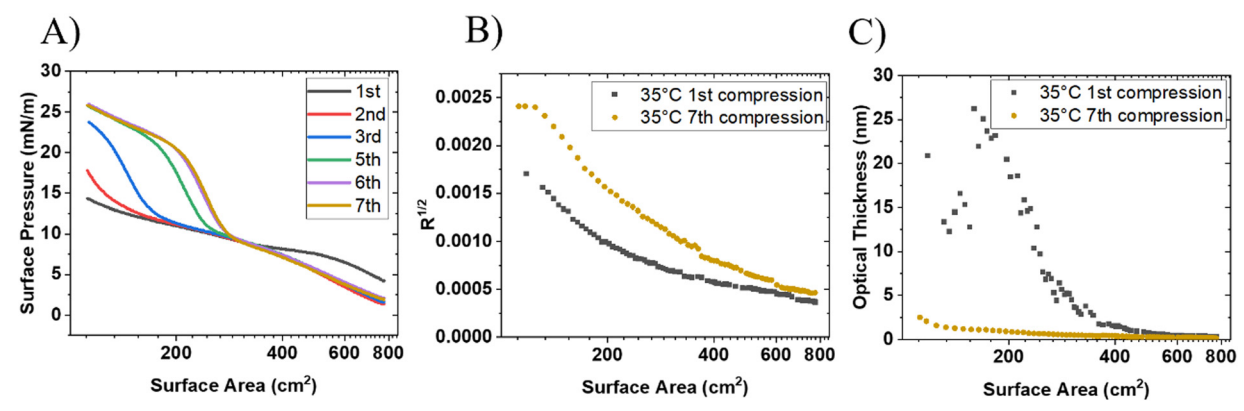


Fig. 5 (A) Compression curves for 7 consecutive compression and expansion cycles at 30 mm min $^{-1}$  for PtBMA-PEG micelles at 35 °C (50  $\mu$ L of 5 mg mL $^{-1}$  solution). (B) Square root of reflectivity for the 1st and 7th compression. (C) Estimated thickness values for the 1st and 7th compression calculated from eqn (1) and (2) using equal and constant mass.

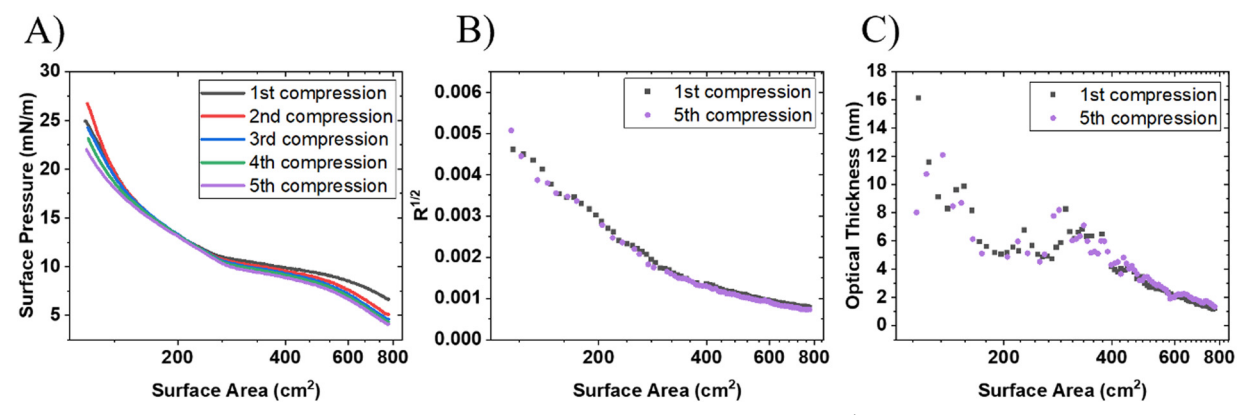


Fig. 6 (A) Compression curves for 7 consecutive compression and expansion cycles at 30 mm min<sup>-1</sup> for PS-PEG micelles at 35 °C (50 μL of 5 mg mL<sup>-1</sup> solution). (B) Square root of reflectivity for the 1st and 5th compression. (C) Estimated thickness values for the 1st and 5th compression calculated from egn (1) and (2) using equal and constant mass

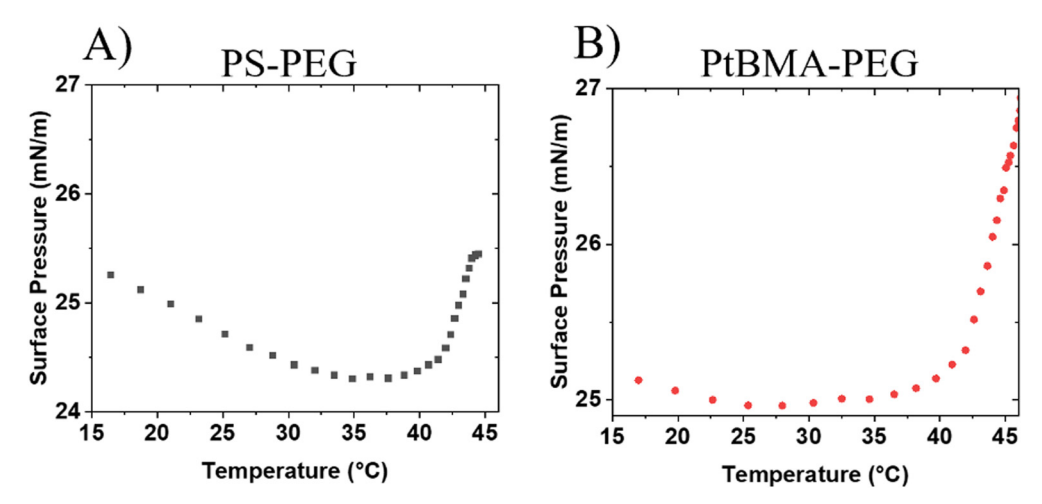


Fig. 7 Constant area heating of micelle films for (A) PS-PEG and (B) PtBMA-PEG. Micelles were spread on the interface at 15 °C, compressed to 25.5 mN m<sup>-1</sup>, and then heated to 45 °C using a heating rate of 1 °C min<sup>-1</sup>

pressure decreases with increasing temperature below core  $T_{g}$ due to a decrease in the PEG corona thickness with increasing temperature which results in a reduction in the overlap of neighboring micelle coronas. A plot of DLS  $D_{\rm h}$  values as a function of temperature, Fig. S4 in ESI,† shows that both PS-PEG and PtBMA-PEG micelle sizes decrease linearly with temperature. At the core outer  $T_{g}$ , the surface pressure increases due to the structural change of the core domain to occupy a larger area such that the separation distance between micelles is decreased and interactions between neighboring PEG coronas is increased. For PS-PEG, the surface pressure increases back to near the original value before heating. For PtBMA-PEG, the surface pressure continues to rise rapidly above 40 °C likely due to the PtBMA domains spreading at the interface. The results agree with the idea of the micelle rearrangement at the outer core  $T_g$  and provide good quantitative agreement with the  $T_g$  values obtained from  $T_2$  <sup>1</sup>H NMR which support the surface pressure vs. temperature measurements being another way to efficiently measure micelle core  $T_g$ .

## 3.4 Implications of the effect of temperature on lung surfactant efficacy

For the lung surfactant application, the ability of the surfactant formulation to produce high surface pressure ( $> 60 \text{ mN m}^{-1}$ ), to respread on the interface and continuously produce high surface pressure during repeated compression (exhalation) and expansion (inhalation) cycles, and satisfying the Laplace stability criterion at the physiological temperature of 37 °C are desired properties. To prevent the collapse of smaller alveoli, it is crucial to control alveolar surface tension  $(\gamma)$  since alveoli with different radii (R) experience varying Laplace pressures  $(\Delta P = \gamma/R)$ . Specifically, the condition  $\partial(\Delta P)/\partial R > 0$  must be maintained, which can be expressed as  $E > \gamma/2$  where E represents the Gibbs modulus ( $\equiv \partial \gamma / \partial \ln(A)$ ) for dilatational deformation.<sup>7</sup> This Laplace stability criterion  $(E > \gamma/2)$  has been proposed as a means to ensure the prevention of alveolar collapse resulting from differences in Laplace pressure. In our analysis of the data, assuming that shear effects are relatively minor in Langmuir trough-based surface tension measurements,

we have applied the same criterion. In order to examine the effect of temperature on each of these qualities, two consecutive compression and expansion cycles were done using a high spreading volume (100 μL of 5 mg mL<sup>-1</sup> micelle solution). This experiment allows compression into the high surface pressure regime, although the high spreading mass leads to some loss of micelles to the subphase.

The isotherm and compressibility modulus from two consecutive compressions at 25 °C, 35 °C, 40 °C and 50 °C are shown for PS-PEG in Fig. 8(A) and (C). The results demonstrate that at 25 °C (below core  $T_{o}$ ), the film produces surface pressure greater than 60 mN m<sup>-1</sup> on the first and second cycle as well as satisfying the Laplace stability criterion for surface pressures greater than 20 mN m<sup>-1</sup>. When the temperature is raised to 35 °C and 40 °C, the maximum pressure is lowered as the isotherm begins to plateau below 60 mN m<sup>-1</sup>. Also, for the 40 °C case, the second compression shows a significant decrease in surface pressure compared to the first compression indicating a loss of material from the interface. This indicates that the contact and deformation of PS domains at high surface pressure, which was proposed to contribute to surface pressure

increase when T > outer core  $T_{\rm g}$ , leads to irreversible loss of material from the interface likely due to the collapse of the PS domains. Despite the 35  $^{\circ}$ C and 40  $^{\circ}$ C cases being at and above the outer core  $T_g$  of 35 °C, there is no significant decrease in the magnitude of the compressibility modulus and the range of Laplace stability. However, when the temperature is raised to 50 °C (well above the mean core internal  $T_{\rm g}$  of 41 °C measured from FCVI) the modulus is significantly reduced indicating a loss of internal rigidity of the micelles. Interestingly, the micelle film respreads very well at 50 °C indicating the more fluid like surface micelles are not expelled from interface at high compression; however, the maximum surface pressure is significantly reduced due to the decreased rigidity of the film.

For PtBMA-PEG micelles, increasing the temperature to very near and slightly above the outer and internal core  $T_g$  leads to a downward shift in the modulus and maximum surface pressure on the first compression, as shown in Fig. 8(B) and (D) due to micelles becoming more deformable. Also, there is a shift to higher surface pressure on the second compression and the development of the pseudo secondary plateau at approximately 25 mN m<sup>-1</sup> which is thought to be due to fusion and respreading

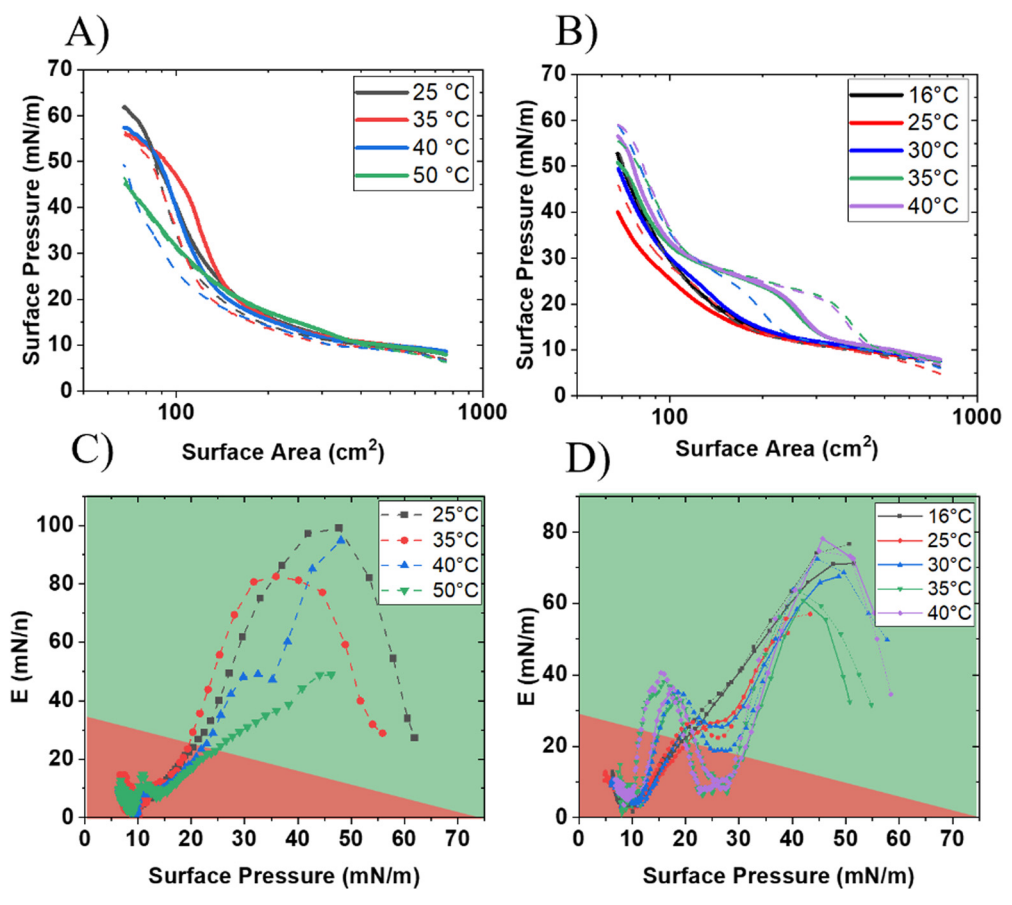


Fig. 8 Compression curves for two consecutive surface pressure—area isotherm compression/expansion cycles for water-spread (A) PS-PEG micelles and (B) PtBMA-PEG micelles (100  $\mu$ L of 5 mg mL $^{-1}$  solution) compressed at 9 mm min $^{-1}$  at various temperatures. The solid lines represent the first compressions, while the dotted lines represent the second compression. Modulus,  $E=-A\frac{\mathrm{d}H}{\mathrm{d}A'}$  plots as a function of surface pressure for (C) PS-PEG and (D) PtBMA-PEG micelles. The green shaded region in (C) and (D) represents the region which satisfies the Laplace stability criterion ( $E > \gamma/2$ ), and the red shaded region is which does not satisfy the stability criterion ( $E < \gamma/2$ ).

Soft Matter

of PtBMA domains as explained earlier. For the 35  $^{\circ}\mathrm{C}$  and 40  $^{\circ}\mathrm{C}$ cases, the spreading alone induces the partial transition from a micelle film to a planar PtBMA film as indicated by the clear emergence of a pseudo-plateau at approximately 25 mN m<sup>-1</sup> on the first compression. The pseudo-plateau can be seen clearly by the local minimum in the modulus plots in Fig. 8(D). This leads to an increase in the maximum surface pressure compared to the 16  $^{\circ}$ C (below core  $T_{\rm g}$  case). The observed increase in surface pressure upon compression beyond the pseudo-plateau can be

attributed to the lateral repulsion between planar PEG brush chains. <sup>28,30</sup> Although the films at 35 °C and 40 °C still produce surface pressure near 60 mN m<sup>-1</sup>, the pseudo-plateau at 25 mN m<sup>-1</sup> causes the film to not satisfy the Laplace stability criterion in the range of 20-30 mN m<sup>-1</sup>. Overall, the region of Laplace instability is shifted from 10-20 mN m<sup>-1</sup> at 16 °C to 20-30 mN m<sup>-1</sup> for 35 °C and 40 °C, which both cover an area range of  $\sim 200 \text{ cm}^2$ . Ultimately, the effects of this shift in Laplace stability range on in vivo efficacy is not yet understood.

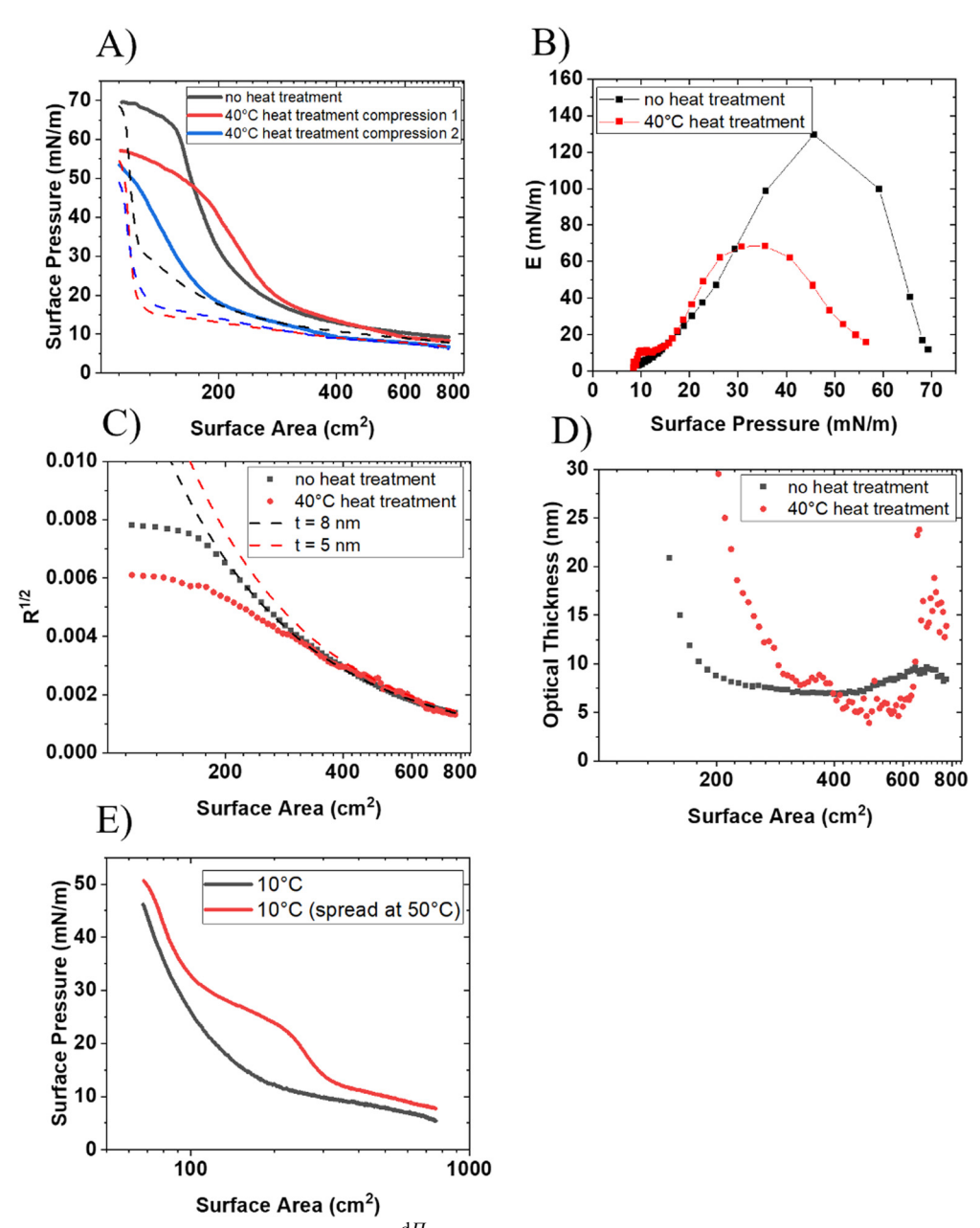


Fig. 9 (A) Surface-pressure area isotherms, (B) modulus,  $E = -A \frac{\mathrm{d} \Pi}{\mathrm{d} A'}$ , plots as a function of surface pressure, (C) square root of reflectivity as a function of surface area measured simultaneously with surface pressure—area isotherms where dashed lines represent the constant thickness and mass model using t = 8 and 5 nm, and (D) estimated thickness from solving eqn (1) and (2) using constant and equal mass for the PS-PEG films with and without heat treatment. Heat treatment was done by first spreading (100 µL of 5 mg mL<sup>-1</sup>) at 25 °C, heating to 40 °C, waiting 15 minutes at 40 °C, and then cooling back to 25 °C. (E) Surface pressure-area isotherms of PtBMA-PEG micelles spread and compressed at 10 °C, and spread at 50 °C, cooled to 10 °C and compressed at 10 °C. The cooling and heating were done at a rate of 1 °C min<sup>-1</sup>.

## 3.5 Irreversibility of structural transition resulting from heating above core $T_{\rm g}$

The proposed changes in surface mechanical behavior have been explained in terms of a structural transition whereby the spherical core domains rearrange when heated above their respective core  $T_g$  values. If this type of structural transition is occurring, then this transition would be expected to be irreversible as the micelle adopts a more energetically favorable state as a result of the increased mobility of the core domain. Therefore, heat treatment experiments were carried out to see if heating above core  $T_{\rm g}$  and then cooling back down below core  $T_{\rm g}$  would result in irreversible changes in surface mechanical behavior.

PS-PEG micelles were spread at the interface at 25 °C, heated to 40 °C and held at this temperature for 15 minutes, cooled back down to 25 °C, and then the surface pressure-area isotherm and QBAM measurements were performed. Comparisons of the isotherms, moduli, reflectivities and calculated thicknesses between non-heat-treated and heat-treated films are shown in Fig. 9(A)-(D). The isotherm for the heat-treated sample more closely resembles that of the isotherm at 40 °C than the isotherm taken at 25 °C. More specifically, the isotherm shows an increase in surface pressure at moderate surface areas (200-400 cm<sup>2</sup>), a deviation from linear modulus vs. surface pressure relationship near 17 mN m<sup>-1</sup>, a plateau in surface pressure below 60 mN m<sup>-1</sup> and poor respreading. Additionally, the thickness is estimated to decrease to t =5 nm at the onset of surface pressure rise. All the features are consistent with an irreversible core transition when heated above core  $T_g$ . Interestingly, the magnitude of the modulus is actually reduced for the heat-treated sample compared to both the non-heat-treated sample and the isotherm conducted at 40 °C. This could be due to the rigid domains not being able to store energy by deformation and instead collapse and are expelled from the interface when they come into contact.

For PtBMA-PEG, a slightly different procedure was carried out whereby micelles were spread at 50 °C and cooled down to 10 °C; the isotherm results comparing heat-treated and nonheat-treated films are shown in Fig. 9(E). The results clearly demonstrate the pseudo-plateau at 25 mN m<sup>-1</sup>, which was the distinguishing feature for micelle films measured at 40 °C, remains after cooling. This also indicates that the transition of PtBMA-PEG micelles is irreversible which is consistent with the core rearrangement hypothesis, and the plateau cannot be explained by thickening/deformation of non-glassy micelles.

## 4. Conclusion

The effect of temperature on the surface-mechanical properties of two different core chemistries has been studied. The results indicate that the increased core flexibility as a result of heating above core  $T_g$  changes the micelle structure at the interface whereby the core domain increases its interfacial area. The effect of physiological temperature (37 °C) on the desired properties for lung surfactant formulation depends on the

chemistry of the core domain. For PS, which has a negative spreading coefficient, increasing the temperature above the core outer  $T_g$  of 35 °C leads to a reduction of maximum surface pressure and worse respreading which are both undesirable. The changes in behavior are proposed to be due to the contact, deformation, and collapse of PS domains at high surface pressure. If the temperature is above the internal core  $T_{g}$ , there is a further reduction in maximum surface pressure due to decreased rigidity of PS domains. For PtBMA-PEG micelles, when the temperature is above the internal core  $T_{\sigma}$  of 29 °C the mobile PtBMA domains spread at the interface which is due to PtBMA having a positive spreading coefficient. The high surface pressure is now caused by the lateral repulsion between planar PEG brush chains which are anchored to a continuous PtBMA film. The formation of a continuous PtBMA film is evident by the presence of pseudo-plateau in surface pressurearea curve causing the film to fall below the Laplace stability criterion in the range of 20-30 mN m<sup>-1</sup>. In vivo studies need to be tested to evaluate what effect this has on efficacy for PLS.

## Conflicts of interest

There are no conflicts to declare.

## Acknowledgements

The authors are grateful for funding from ACS PRF (60233-ND7), NSF (IIP-2036125, CBET-2211843), and Spirrow Therapeutics. The authors also acknowledge support from the Purdue University Center for Cancer Research (PCCR) via an NIH NCI grant (P30 CA023168), which supports the campus-wide NMR shared resources that were utilized in this work. The authors acknowledge Fig. 2 and 4 and the Graphical Abstract were made using Biorender.com.

## References

- 1 H. C. Kim, M. V. Suresh, V. V. Singh, D. Q. Arick, D. A. Machado-Aranda, K. Raghavendran and Y.-Y. Won, ACS Appl. Bio Mater., 2018, 1, 581-592.
- 2 D. J. Fesenmeier, M. V. Suresh, S. Kim, S. Park, K. Raghavendran and Y.-Y. Won, ACS Biomater. Sci. Eng., 2023, 9, 2716-2730.
- 3 J. Máca, O. Jor, M. Holub, P. Sklienka, F. Burša, M. Burda, V. Janout and P. Ševčík, Respir. Care, 2017, 62, 113-122.
- 4 P. Schousboe, A. Ronit, H. B. Nielsen, T. Benfield, L. Wiese, N. Scoutaris, H. Verder, R. M. G. Berg, P. Verder and R. R. Plovsing, Sci. Rep., 2022, 12, 4040.
- 5 S. Tasaka, Acute Respiratory Distress Syndrome: Advances in Diagnostic Tools and Disease Management, Springer, 2022, pp.33-52.
- 6 A. Dushianthan, R. Cusack, V. Goss, A. D. Postle and M. P. W. Grocott, Crit. Care, 2012, 16, 238.
- 7 S. Barman, M. L. Davidson, L. M. Walker, S. L. Anna and J. A. Zasadzinski, Soft Matter, 2020, 16, 6890-6901.

- 8 D. J. Fesenmeier, S. Park, S. Kim and Y.-Y. Won, J. Colloid Interface Sci., 2022, 617, 764-777.
- 9 S. Kim, S. Park, D. J. Fesenmeier, T. Jun, K. Sarkar and Y.-Y. Won, Langmuir, 2023, 39, 13546-13559.
- 10 H. C. Kim, D. Q. Arick and Y.-Y. Won, Langmuir, 2018, 34, 4874-4887.
- 11 H. C. Kim, Y. H. Choi, W. Bu, M. Meron, B. H. Lin and Y. Y. Won, Phys. Chem. Chem. Phys., 2017, 19, 10663-10675.
- 12 H. C. Kim, H. Lee, H. Jung, Y. H. Choi, M. Meron, B. Lin, J. Bang and Y.-Y. Won, Soft Matter, 2015, 11, 5666-5677.
- 13 H. W. Park, J. Choi, K. Ohn, H. Lee, J. W. Kim and Y. Y. Won, Langmuir, 2012, 28, 11555-11566.
- 14 S. Kim, M. Lee, H. Chang Kim, Y. Kim, W. B. Lee and Y.-Y. Won, Macromolecules, 2023, 56, 6290-6304.
- 15 C. J. Ellison and J. M. Torkelson, Nat. Mater., 2003, 2, 695-700.
- 16 D. J. Fesenmeier, H. C. Kim, S. Kim and Y.-Y. Won, Macromolecules, 2023, DOI: 10.1021/acs.macromol.3c01486.
- 17 B. H. Cao and M. W. Kim, Faraday Discuss., 1994, 98, 245-252.
- 18 G. Fleer, M. C. Stuart, J. M. Scheutjens, T. Cosgrove and B. Vincent, Polymers at interfaces, Springer Science & Business Media, 1993.

- 19 M. Rubinstein and R. H. Colby, Polymer physics, Oxford university press, New York, 2003.
- 20 K. N. Witte, S. Kewalramani, I. Kuzmenko, W. Sun, M. Fukuto and Y. Y. Won, Macromolecules, 2010, 43, 2990-3003.
- 21 R. Vilanove and F. Rondelez, Phys. Rev. Lett., 1980, 45, 1502-1505.
- 22 S. Kawaguchi, G. Imai, J. Suzuki, A. Miyahara, T. Kitano and K. Ito, Polymer, 1997, 38, 2885-2891.
- 23 J. G. Fernsler and J. A. Zasadzinski, Langmuir, 2009, 25, 8131-8143.
- 24 J. H. Fendler, Adv. Mater., 1996, 8, 260.
- 25 S. Kim, S. Park, D. J. Fesenmeier, T. Jun, K. Sarkar and Y.-Y. Won, Langmuir, 2023, 39(38), 13546–13559.
- 26 S. Wu, J. Polym. Sci., Part C: Polym. Symp., 1971, 34, 19-30.
- 27 G. T. Gavranovic, J. M. Deutsch and G. G. Fuller, Macromolecules, 2005, 38, 6672-6679.
- 28 K. N. Witte, J. Hur, W. Sun, S. Kim and Y. Y. Won, Macromolecules, 2008, 41, 8960-8963.
- 29 H. Lee, D. H. Kim, H.-W. Park, N. A. Mahynski, K. Kim, M. Meron, B. Lin and Y.-Y. Won, J. Phys. Chem. Lett., 2012, 3, 1589-1595.
- 30 H. C. Kim, H. Lee, J. Khetan and Y. Y. Won, Langmuir, 2015, 31, 13821-13833.